



Formation of weak and strong Brønsted acid sites during alkaline treatment on MOR zeolite



N. Chaouati^{a,b}, A. Soualah^b, I. Hussein^a, J-D. Comparot^a, L. Pinard^{a,*}

^a Université de Poitiers, CNRS UMR7285, Institut de Chimie des Milieux et Matériaux de Poitiers, B27, TSA 51106, 4 rue Michel Brunet, 86073 Poitiers CEDEX 9, France

^b Laboratoire de Physico-Chimie des Matériaux et Catalyse, Faculté des Sciences Exactes, Université de Bejaia, 06000, Bejaia, Algérie

ARTICLE INFO

Article history:

Received 25 May 2016

Received in revised form 28 July 2016

Accepted 3 August 2016

Available online 4 August 2016

Keywords:

Desilication

Hierarchization

CO

Pyridine

M-xylene isomerization

ABSTRACT

Aluminum rich mordenite zeolite ($\text{Si}/\text{Al} = 10$) was hierarchized by using mild (0.2 M NaOH and 70 °C) and severe (0.4 M NaOH and 85 °C) alkaline treatments. The textural characterization was made by nitrogen adsorption. Acidic properties, i.e. nature (N), concentration (C), strength (S), accessibility (A) and location (L), were drawn from adsorption of two probes molecules followed by infrared spectroscopy: pyridine for N, C, L and S properties while CO for N and S properties. The catalytic model reaction of *m*-xylene transformation was also used to determine C, S and L properties. The severe alkaline treatment promoted (i) silicon extraction of zeolite framework, without considerable loss of crystallinity, (ii) creation of intra-crystal mesopore and widening of micropore diameter due to formation of interconnection between main canals, and (iii) accessibility of Brønsted acid sites (BAS) located in side pockets. The silicon removal is inevitably followed by formation of extraframework aluminum species (EFAL) that leads to formations of Lewis acid sites, weak extraframework BAS and very strong BAS due to interaction between EFAL with the bridged hydroxyl, evidenced by a correlation between turnover frequency in *m*-xylene transformation and concentration of LAS.

© 2016 Published by Elsevier B.V.

1. Introduction

Zeolites are some of the most catalysts used in industrial process (oil refining, petrochemicals and chemicals manufacturing) and their applications grow steadily [1–3]. In addition to a unique regular microporosity and strong acid sites, their properties can be controlled either during their synthesis or by post-synthesis treatments [4]. Among the main used zeolites, mordenite is used in some major petrochemical processes such as isomerization of C_8 aromatics, hydroisomerization of light alkanes and cumene synthesis [5–7].

Dealumination post-synthesis treatment is usually performed on zeolites to increase stability, activity, thermal stability and control concentration of Brønsted acid sites (BAS) [8]. Zeolite dealumination is a simple and efficient tool to adjust meso/micropore network [7] in detriment to acidity owing to Al removal. Impact of dealumination on zeolite acidity has been widely studied during the last decades. Enhancement in activity on steamed mordenites was observed by Mirodatos and Barthomeuf [9,10]. This benefit effect is

only observed on mildly steamed zeolites, since more severe dealumination leads to a considerable diminution of acid sites and hence to activity [11]. It has been proposed that this higher activity results from interplay between active sites rather than merely a decrease in the concentration of framework aluminum [12]. Henriques et al. [13], explain the higher activity in *o*-xylene transformation on dealuminated modrenite by (i) the increase of accessibility of acid sites, owing to the presence of secondary mesoporous system and by (ii) the generation of very strong Brønsted acid sites (BAS) by interaction of Lewis acid sites with BAS [14,15]. Role of extra-framework aluminum (EFAL) was evidenced by showing on series of realuminated mordenites that supplementary activity is generated when introduced Al is on non-framework position [16]. More than that, Hong et al. [17] demonstrate that there is a correlation between the initial rates of *o*-xylene conversion per Brønsted acid site and the number of available Lewis acid sites.

The other post-synthesis method, more efficient to generate mesoporosity is desilication by alkaline treatment. Contrary to dealumination studies, there is less attention concerning the impact of such modification on acidity. In the majority of cases, catalytic activity data is usually interpreted in term of textural modifications by admitting minor modification of the acidity [18]. Only the increase in acid density and the decrease in acid strength owing to

* Corresponding author.

E-mail address: ludovic.pinard@univ-poitiers.fr (L. Pinard).

Table 1
Acid and alkaline treatment conditions.

Treatment	Acid	Alkaline	
Agent	HCl	NaOH	NaOH
Concentration (M)	0.5	0.2	0.4
Temperature (°C)	30	70	85
Time (min)	10	120	120

diminution of Si/Al molar ratio were highlighted [18]. Paixao et al. [19], explained the decrease on *m*-xylene conversion on desilicated mordenite, by a loss of concentration of acid sites. But the same authors, in another study, observed no change in acidic properties after alkaline treatment of mordenite [20].

The aim is to study the impact of desilication on the acidity of mordenite zeolite. For this purpose, acidity will be characterized by classical physicochemical methods such adsorption of probe molecules (Pyridine and CO) followed by infra-red spectroscopy and model reaction (*xylene transformation*).

2. Experimental

2.1. Alkaline and acid treatments of HMOR zeolite

The zeolite used as a starting material was a commercial protonic mordenite (MOR, Süd chemie) with a molar ratio Si/Al of 10. Alkaline treatment was carried out using NaOH as desilicating agent following operating conditions reported in Table 1. Briefly, 10 g of MOR were stirred at 400 rpm in 300 ml alkaline solution (0.2–0.4 M) at 70 °C and 85 °C respectively for 2 h. Then, zeolite suspension was centrifuged (6000 rpm) after being cooled down in ice–water mixture. The decantation of the liquid was followed by re-suspension with demineralized water. This procedure was repeated until pH was 7. Samples were subsequently treated with 0.5 M of HCl under stirring at 30 °C for 10 min using the proportion of 10 ml per gram of sample (Table 1). All samples were converted into their correspondent protonic form by three consecutive exchanges with 2 M, NH₄NO₃ using the proportion: 20 cm³/g of zeolite. The exchange was carried out at 60 °C for 4 h. After a careful wash up to pH 7, solid was calcined under air flow (100 ml min⁻¹/g of zeolite) at 550 °C for 5 h.

2.2. Physicochemical characterization

X-ray diffraction (XRD) data were acquired on a PAN analytical (XPert Pro MPD) diffractometer over a 5°–50° 2θ range using the CuKα radiation ($\lambda = 154.05 \text{ pm}$). Samples were characterized by transmission electronic microscopy (TEM) using a Philips CM 120 microscope equipped with a LaB₆ filament. Chemical composition of samples was measured by X-ray fluorescence (XRF) and by using inductively coupled plasma–atomic emission spectroscopy (ICP-AES) on an Optima 4300 DV (Perkin–Elmer). External Si/Al molar ratio was measured by XPS using a Kratos Axis Ultra DLD instrument.

A Micromeritics ASAP 2000 gas adsorption analyzer was used for nitrogen sorption measurements. Prior to measurement, samples were outgassed at 90 °C for 1 h and 350 °C for 10 h. Specific surfaces areas were determined from the BET equation. Total pore volume corresponds to the nitrogen volume adsorbed at $P/P_0 = 0.96$ and *t*-plot method was used to distinguish micropores from mesopores. Mesopore size distribution was estimated by the BJH method.

2.3. Acidity characterization by adsorption of probe molecule followed by IR

The possible modifications in acidic properties of starting material (nature, concentration and strength) caused by the different treatments were studied by using adsorption of two probes molecules followed by infrared spectroscopy (FTIR). Adsorption of pyridine at 150 °C measures the amounts of Brønsted and Lewis sites by integrating the band areas at 1545 cm⁻¹ and 1454 cm⁻¹ respectively and by using extinction coefficients given in Ref. [21]. Adsorption of carbon monoxide at –100 °C evaluates acid strength of hydroxyl group by measuring value of OH band red-shift [22]. The infrared spectra were recorded in a Nicolet Magna 550-FT-IR spectrometer with a 2 cm⁻¹ optical resolution. The zeolites were first pressed into self-supporting wafers (diameter: 1.6 cm, 18 mg) and pretreated from room temperature to 500 °C (heating rate of 1.5 °C/min for 5 h under a pressure of 10⁻⁶ Torr) in a IR cell connected to a vacuum line.

2.4. Acidity characterization by model reaction: *m*-xylene transformation

The conversion of *m*-xylene (Aldrich, 99% pure) was performed at atmospheric pressure in a fixed bed reactor at 350 °C, with a N₂/reactant molar ratio of 13.5 and a contact time (1/WHSV) of 0.006 h. Before testing, catalysts were compacted, crushed and sieved to obtained homogeneous particles (0.2–0.4 mm). Samples were pre-treated at 450 °C under air flow (60 ml min⁻¹) over night. Reaction products were analyzed online by gas chromatography using a VARIAN 3800 gas chromatograph equipped with a FID detector using a 60 m fused silica J&W DB WAX capillary column.

2.5. Spent catalyst characterization

Coke amount was determined with a SDT Q600 TA thermogravimetric analyzer by heating up to 900 °C (20 °C min⁻¹) under a 100 ml min⁻¹ (O₂ 10%/He) flow. Residual porosity was measured by N₂ adsorption and residual acidity by pyridine adsorption followed by FTIR.

3. Results and discussion

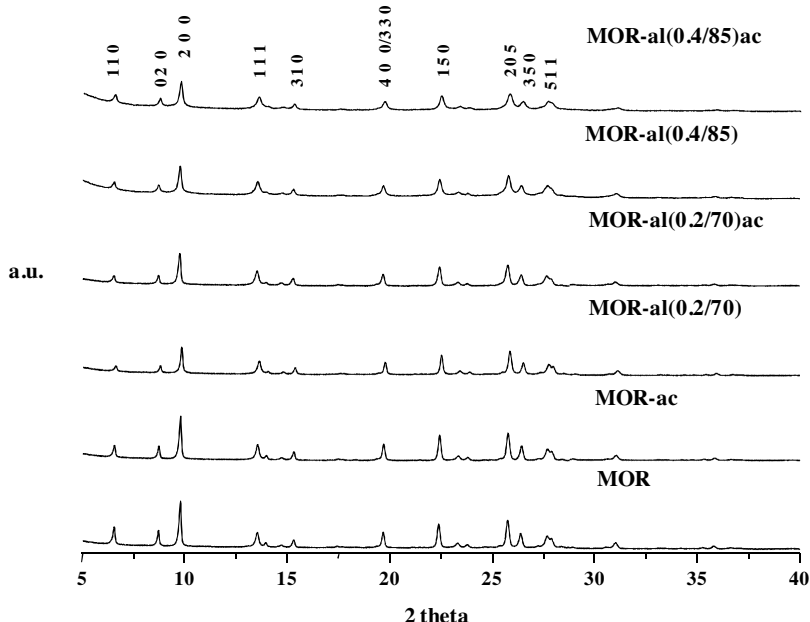
3.1. Physicochemical characterization

The physicochemical properties of the parent zeolite (MOR) and its derivatives (crystal size, crystallinity, external and BET surfaces, micropore and mesopore volumes) are quoted in Table 2. Samples are designated as follows: the values in brackets are sodium hydroxide concentration (M) and temperature (°C) used for alkaline treatment; the subscript:-ac indicates a subsequent acid leaching. The powder XRD patterns, displayed in Fig. 1, show the preservation of mordenite structure upon alkaline and acid treatments. On the other hand, desilication led to a loss of crystallinity which can be estimated (from the ratio between the areas of all diffraction peaks of the samples and of the starting material) to ca 20 and 30%. The crystallinity slightly increased after acid leaching owing to the dissolution of amorphous species created during alkaline treatment (EFAL). The nitrogen adsorption-desorption isotherm of starting material displays an isotherm of type I (characteristic of a microporous structure) and a hysteresis loop at high relative pressure ($P/P_0 > 0.9$). This small hysteresis is due to mesopores formed by the agglomeration of zeolite crystals [19]. Indeed, TEM micrograph on Fig. 3 shows that MOR crystals are strongly aggregated and that the void between them can be assimilated to inter-granular mesopores. The mild desilication conditions were not enough to create significant change in porosity (Table 2). On the other hand, both a higher

Table 2

Textural and structural properties of MOR series.

	unity	MOR	MOR-ac	MOR-al(0.2/70)	MOR-al(0.2/70)ac	MOR-al(0.4/85)	MOR-al(0.4/85)ac
Crystal size ^a	nm	100–500	100–500	100–500	100–500	–	–
Crystallinity ^b	%	100	100	78	81	72	77
S_{BET} ^c	$m^2 g^{-1}$	524	530	544	649	544	558
S_{ext} ^d	$m^2 g^{-1}$	23	17	72	85	130	170
$V_{ultramic.}$ ^d	$cm^3 g^{-1}$	0.20	0.20	0.19	0.21	0.17	0.18
$V_{totalmic.}$ ^e	$cm^3 g^{-1}$	0.20	0.21	0.22	0.24	0.20	0.21
V_{meso} ^f	$cm^3 g^{-1}$	0.06	0.05	0.14	0.12	0.23	0.26
D_p (BJH) ^g	nm	–	–	4.20	4.20	5.25	5.25
D_p (TEM) ^h	nm	–	–	5	5	<10	<10

^a Apparent size determined by using SEM and TEM images (Fig. 3).^b calculated from XRD.^c Specific surface area measured by BET.^d External surface and micropore volume using *t*-plot method.^e Total microporous volume estimated by DR method.^f Mesopore volume = $V_{total} - V_{micro}$ (V_{total} : determined from the adsorbed volume at $p/p_0 = 0.96$).^g Pore size distribution estimated by BJH method and.^h according to TEM images (Fig. 3).**Fig. 1.** X-ray diffraction patterns of MOR series.

temperature and a higher NaOH concentration were necessary to generate a well pronounced hysteresis loop, which is typical of presence of mesopores (Fig. 2). During alkaline treatment, the most important textural modification is the generation of mesopores ($V_{meso} = 0.26 \text{ cm}^3 \text{ g}^{-1}$), that automatically leads to an increase of external surface ($S_{ext} = 170 \text{ cm}^2 \text{ g}^{-1}$). TEM images in Fig. 3 confirm the presence of intra-crystal mesopores with an average diameter, estimated by BJH method, to ca 5 nm (Table 2 and Fig. 2). The mesopore distribution seems more homogeneous by using a severe alkaline treatment than a mild one. The used operating condition for acid leaching (Table 1) did not change the textural properties of the starting material (Table 2); it is too mild to cause a dealumination of the MOR zeolite, but sufficient to dissolve amorphous species formed during alkaline treatment.

3.2. Acidity characterization by pyridine adsorption at 150 °C

The acidic properties of zeolites were characterized by XRF, ICP, XPS, FTIR and adsorption of pyridine followed by FTIR. Their main features are summarized in Table 3. Global molar Si/Al ratio

decreased after alkaline treatment owing to a preferential silicon extraction, and increased again after acid leaching due to a selective dissolution of extra-framework Al species (EFAL). The differences between global and external molar Si/Al ratios were similar with all samples (except with MOR-al(0.2/70)ac)), meaning firstly an homogenous distribution of Al on the starting material and secondly that silicon extraction occurs both on external surface and inside zeolite crystal. The low value of $(\text{Si}/\text{Al})_{surf}$ of MOR-al(0.4/85) is probably due to a large amount of amorphous alumina on external surface as indicates the too low global molar Si/Al ratio (6.0). The framework Si/Al molar ratios drawn from TOT bands (SSI, [20]), were similar whatever the used treatments, as a consequence the theoretical concentrations of Brønsted acid sites were close on all samples, i.e. $\sim 1300 \mu\text{mol g}^{-1}$. On the other hand, the number of EFAL atom per unit cell of zeolite was function on the used protocol: alkaline treatment caused an increase of EFAL up to 2.7, while the subsequent acid leaching dissolved them.

The hydroxyl stretching vibration region of IR spectra before (continuous line) and after (dotted line) adsorption of pyridine is given in Fig. 4. MOR exhibits an intense band at 3607 cm^{-1}

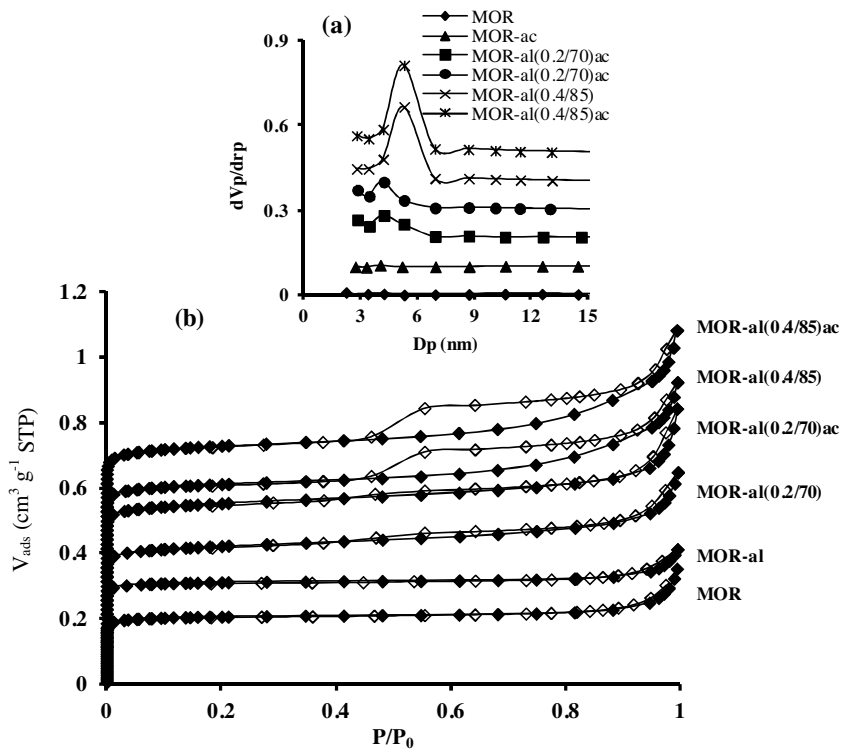


Fig. 2. (a) BJH pore size distribution of different samples (shift 0.1), (b) N_2 adsorption (open symbols) and desorption (solid symbols) isotherms at 77 K of MOR series (isotherms are shifted by +100).

Table 3
Acidic proprieties of MOR series.

	unity	MOR	MOR-ac	MOR-al(0.2/70)	MOR-al(0.2/70)ac	MOR-al(0.4/85)	MOR-al(0.4/85)ac
Si/Al _{global} ^a	molar	10.0	10.3	8.1	9.2	6.0	9.8
Si/Al _{framework} ^b	molar	11.6	11.5	11.3	11.9	10.7	10.9
Si/Al _{external} ^c	molar	12.4	–	8.4	15.7	5.7	10.9
[Na] ^d	wt.%	0.04	0.05	0.04	0.05	0.04	0.04
[H ⁺] _{theoretical} ^d	$\mu\text{mol g}^{-1}$	1329	1333	1352	1289	1417	1333
EFAL ^e	atom per cell	0.6	0.4	1.4	1.0	2.7	0.4
[PyH ⁺] ^f	$\mu\text{mol g}^{-1}$	1056	968	621	680	337	533
[PyL] ^f	$\mu\text{mol g}^{-1}$	31	38	100	84	133	101
PyAcc ^g	%	75	78	93	95	65	80

^a Measured by XRF and ICP.

^b According to TOT band at 1080–1200 cm^{-1} using the correlation given in ref [20].

^c Determined by XPS.

^d Calculated from framework Al.

^e Extra-framework Al calculated from a and b.

^f Measured by pyridine adsorption on Brønsted (PyH⁺) and Lewis (PyL).

^g Drawn from subtraction of IR spectra of OH band before and after pyridine adsorption.

attributed to bridging hydroxyls groups (i.e. acidic hydroxyl groups) and a small band at 3744 cm^{-1} assigned to stretching vibrations of terminal silanol (SiOH). Alkaline treatment led to a decrease of the intensity of the main band concomitant both of an increase of SiOH band and of the appearance of a small band at 3660 cm^{-1} , assigned to EFAL species. The decrease of intensity of bridging hydroxyls groups could be due in part to the loss of zeolite crystallinity (20 and 30% as shown previously). After pyridine adsorption, the bands of SiOH and EFAL species remain almost unchanged for all samples, as these groups do not present an acid character. On the other hand, the main band associated to Brønsted acid sites (BAS) decreases significantly but not totally. 75% of acid sites were probed by pyridine (PyAcc, Table 3), suggesting that 3/4 of acid sites are located in the main channels and 1/4 in the side pockets of MOR structure; this repartition is in accordance with the open literature [23,24]. The alkaline treatment makes accessi-

ble one part of BAS located in the side pockets, but a subsequent acid leaching is necessary in order to totally benefit of this supplementary accessibility. Indeed, EFAL species generated during alkaline treatment can block access of pyridine to these new sites and even to those located in the main channel (Table 3). The concentration of Brønsted and Lewis acid sites (BAS and LAS) were carried out using the IR bands 1545 and 1454 cm^{-1} (Table 3). On MOR sample the number of BAS probed by pyridine corresponds to theoretical acidity multiplied with the percentage of accessible acidic hydroxyl groups. On the other hand, some important discrepancies between the theoretical and measured acidities (even in taking account the crystallinity) appear after alkaline treatment. These differences cannot simply explain by a blockage of access to BAS by EFAL species, but by a modification of acidic strength of Brønsted acid sites, as that was proposed by some authors [19,25].

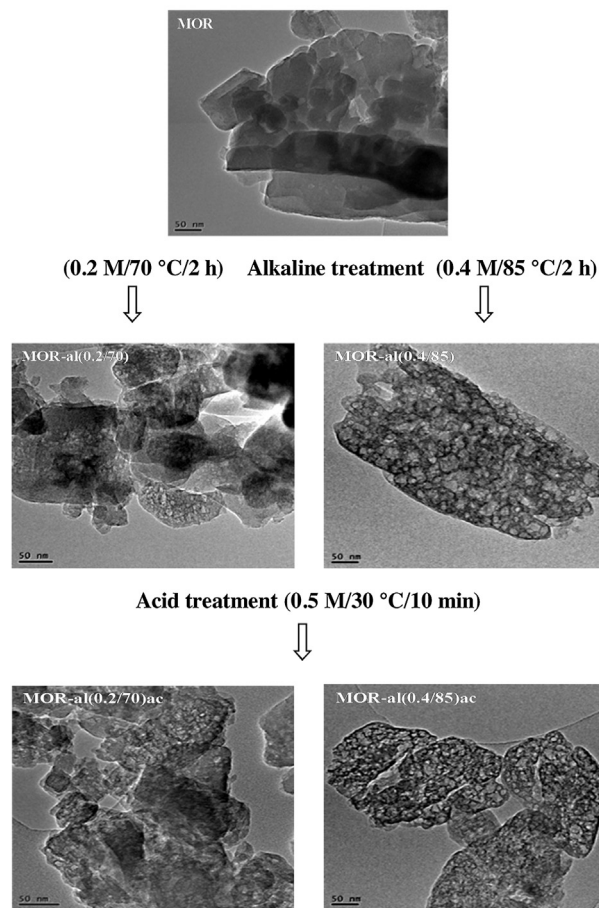
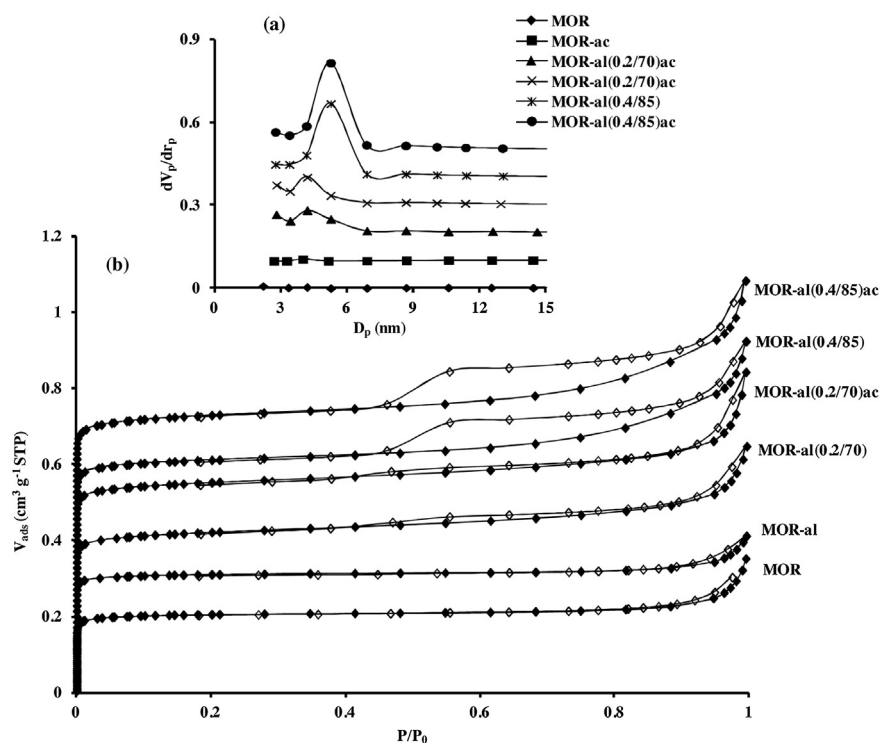


Fig. 3. TEM micrographs of MOR series.

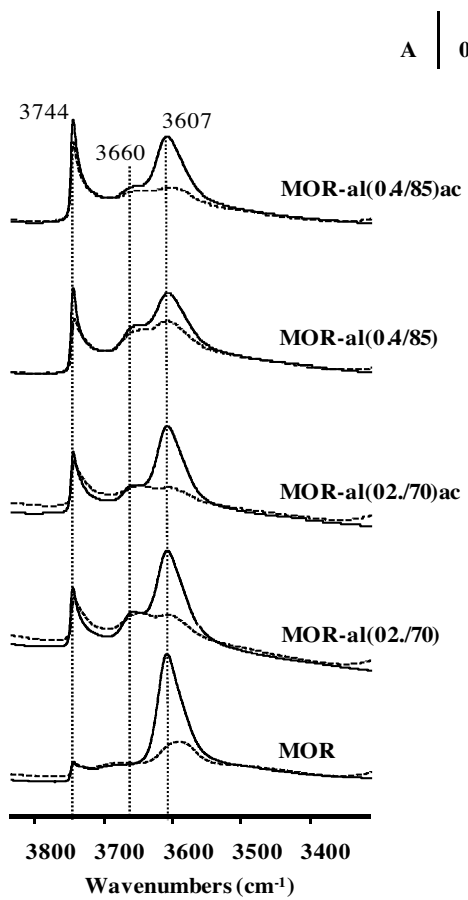


Fig. 4. IR spectra of MOR series before (continuous line) and after (dotted line) pyridine adsorption at 150 °C.

3.3. Characterization of acidity by CO adsorption at low temperature

Carbon monoxide is a slightly basic molecule of electronic structure, which is extremely sensitive not only to the chemical properties of the adsorption centres but also to their geometrical configuration [26]. The small kinetic diameter of CO allows probing all BAS on the MOR zeolite structure, even those located on side pockets. This probe molecule, ideal to study the strength of zeolite acid site [27], forms hydrogen bond with acidic OH groups of zeolite through the lone pair of electrons located on carbon atom. Resulting elongation of O–H is observed in infrared spectrum as lowering of the stretching frequency of hydrogen-bonded OH group, which, in turn depends primarily on the intrinsic acidity of particular hydroxyl group [28]. Fig. 5a presents subtracted IR spectra obtained after successive introduction of CO doses: 50, 100, 200, 300, 400, 500 mbar, and just before appearance of CO in gas phase i.e. saturation of the zeolite surface. On the MOR sample, interaction of CO with SiOH are limited, while with bridging hydroxyl groups that leads to a decrease of intensity of band at 3610 cm^{-1} concomitant of the appearance of a broad band centered around 3300 cm^{-1} . The deconvolution of this band, shown in Fig. 5b, allows discriminating two types of BAS. A simple reasoning would be to assign the first red-shift to interaction of CO ($\Delta\nu_{\text{OH}1} = 322\text{ cm}^{-1}$, Table 4) with OH located in main channel and the second ($\Delta\nu_{\text{OH}2} = 175\text{ cm}^{-1}$) with OH located in the side pockets. But, the proportion of these two families (9/1) is 3 times higher than this found with pyridine (3/1), that means that the two families cannot be classified in terms of location but of strength. It is possible to calculate protonic affinity (PA) from $\Delta\nu_{\text{OH}}$ by using the equa-

tion of Paukstis and Yurchenko [28]; the higher the proton affinity value, the weaker the strength of acid sites. Thus on MOR sample, OH₁ are stronger ($\text{PA}_1 = 1145\text{ kJ mol}^{-1}$) than OH₂ ($\text{PA}_2 = 1262\text{ kJ mol}^{-1}$). The value of PA₂ is similar to that found on a silica-alumina [29]. The strengths of OH₁ and OH₂ stay unchanged regardless of treatment carried out ($\text{PA}_1 \sim 1150\text{ kJ mol}^{-1}$), contrariwise to their proportions; the percentage of OH₁ decreases after alkaline treatment but it is restored after acid leaching. This show that EFAL species formed during desilication are not only Lewis acid sites but also have OH group with acid properties similar to silica alumina.

3.4. Characterization of acidity by model reaction: *m*-xylene conversion

The effect of alkaline treatment on the acidic properties of MOR was evaluated by catalytic reaction of transformation of *m*-xylene, which is commonly used as a model reaction to characterize acidity [30]. At 350 °C, the main reactions are *m*-xylene monomolecular isomerization (I) onto *o*- and *p*-xylene and disproportionation (D) into toluene (T) and trimethylbenzene (TMB). The side reactions are transalkylation between alkylaromatics as indicated by presence of low amounts of benzene and tetramethylbenzene (TeMB), and bimolecular *m*-xylene isomerization whose contribution in isomers products can reach 16%. Fig. 5 shows the evolution of conversion, and molar yield into I and D products as a function of time-on-stream (TOS). All samples follow the same pattern of deactivation, i.e. a fast initial decrease of the conversion related to the decrease of yield into D products, the yield into I products staying quasi stable. The active sites in disproportionation are sensible to deactivation contrariwise to these in isomerization. The D reaction passes through the formation of a reactional intermediate, biphenylmethane, known to be a coke precursor [31] (Fig. 6).

All samples display same initial conversion (ca 40%) except on MOR-al(0.2/70) (Table 5). The initial activities per accessible acid sites probed by pyridine, commonly named: turn over frequency (TOF), increase after desilication and decrease after the subsequent acid leaching. Such changes cannot be related to modification in textural properties of materials but in the strength of acid sites. TOF is both proportional and inversely proportional to the concentrations of LAS and BAS, respectively (Fig. 7). Hong et al. [17], also showed that initial activity per Brønsted site was proportional to the number of Lewis sites and they concluded to a synergic enhancement of the acidity by interaction between Brønsted and Lewis centers. This synergic effect is related to intensification of the strength of BAS [17]. Characterization of acidity by model reaction allow to highlight the exaltation of BAS by EFAL at the difference of the adsorption of probe molecules followed by infrared spectroscopy, and more particular CO which is a technique more adapted to the characterization of weak acid sites.

The Table 6 displays the initial product distribution at isoconversion (X=60%) on the MOR catalyst series. Initial selectivity in isomers, expressed by I/D ratio, reduced on all treated materials. Whatever post-treatment carried out, p/o and T/TMB ratios stay constant and close to 1, implying no diffusion limitation of xylene isomers and that T and TMB results from xylene disproportionation. Relative amounts of the bulkiest isomers (1–3 and 1,3,5-TMB) gives information on the available space near acidic sites owing to steric constraint for the formation of corresponding transition states [32]. Initial ratio of 1–3/1,3,5-TMB slightly decreases after a mild alkaline treatment, stays constant after a subsequent acid leaching, indicating a moderate modification of microporous shape. A more severe desilication condition causes an increase of ratio between TMB isomers, owing to the diminution of vacant space near the acid site by EFAL species; their dissolution by acid washing leads to a strong decrease of TMB ratio up to a value obtained on FAU zeolite (0.27) [32]. In addition to the formation of mesopores, severe alkaline

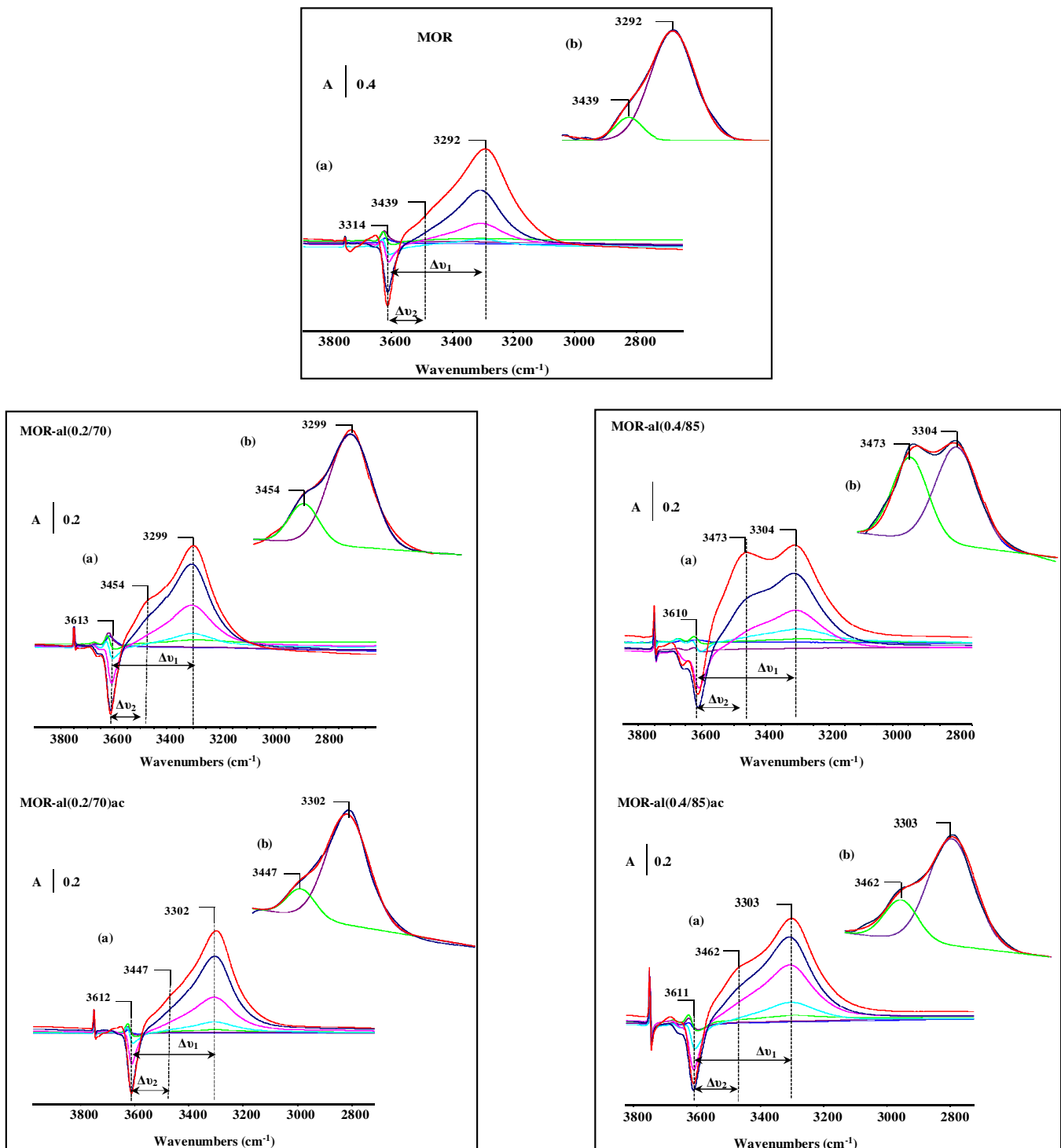


Fig. 5. IR bands resulting from CO adsorption at low temperature of MOR series: (a) subtracted spectra with background after adsorption of gradual amounts of CO 50, 100, 200, 300 400, 500 mbar and up to saturation (b) deconvolution of perturbed OH band after CO adsorption.

Table 4

Values of OH groups frequency downshift ($\Delta\nu$) due to interaction with CO and proton affinities of different population of protonic sites.

	$\nu_0(\text{cm}^{-1})$	$\nu_1(\text{cm}^{-1})$	$\nu_2(\text{cm}^{-1})$	$\Delta\nu_1(\text{cm}^{-1})$	$\Delta\nu_2(\text{cm}^{-1})$	$\text{PA}_1^{\text{a}}(\text{kJ mol}^{-1})$	$\text{PA}_2^{\text{a}}(\text{kJ mol}^{-1})$	$A_1^{\text{b}}\%$	$A_2^{\text{b}}\%$
MOR	3614	3292	3439	322	175	1145	1262	89	11
MOR-al(0.2/70)	3613	3299	3454	314	159	1150	1280	75	25
MOR-al(0.2/70)ac	3612	3302	3447	310	165	1152	1273	86	14
MOR-al(0.4/85)	3610	3304	3473	306	137	1154	1309	60	40
MOR-al(0.4/85)ac	3611	3303	3462	308	149	1153	1293	78	22

^a Proton affinity of the different population of sites calculated according to: $\text{PA} = 2254.8 - 442.5 \log((\Delta\nu))$.

^b Population of acid sites (A_1 and A_2) corresponding to low ($\Delta\nu_1 = \nu_0 - \nu_1$) and high ($\Delta\nu_2 = \nu_0 - \nu_2$) downshift of OH band estimated after deconvolution of band centered at 3300 cm^{-1} .

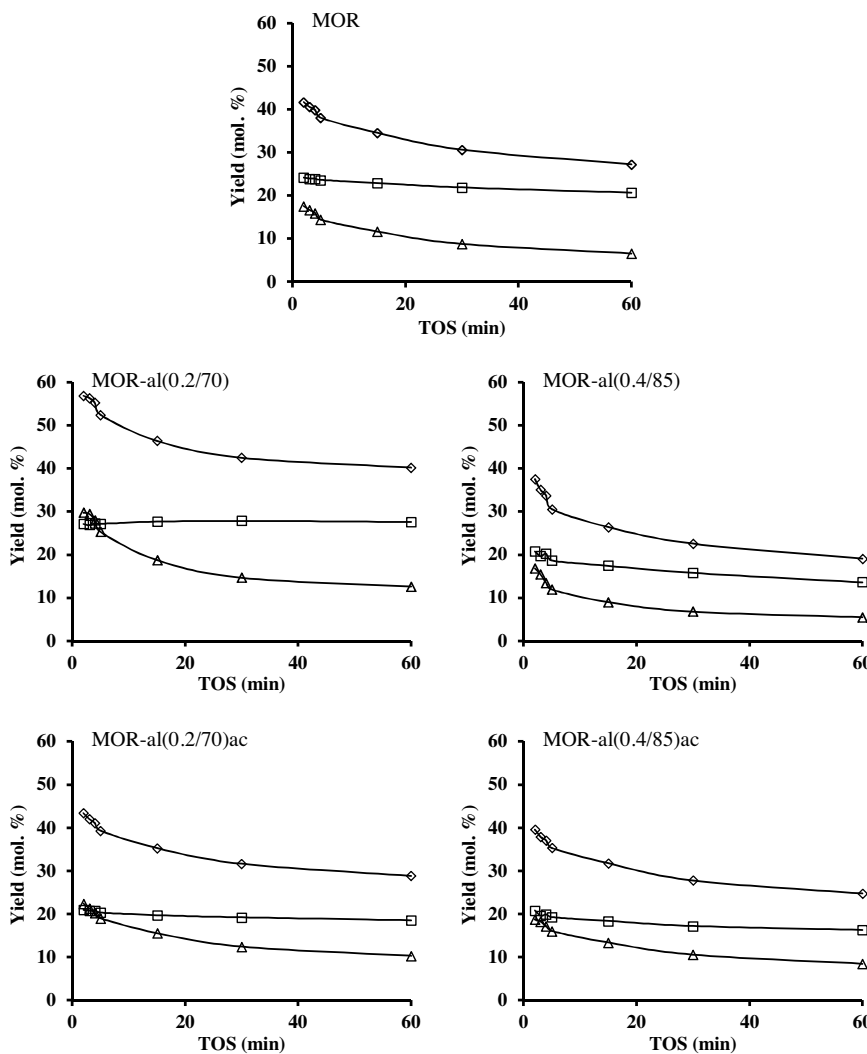


Fig. 6. m-Xylene conversion (\diamond) and yields in disproportionation (Δ) and isomerization (\square) products as a function of time on stream.

Table 5

Conversion, activity and turn-over-frequency of transformation of m-xylene on the fresh (time-on-stream, TOS = 2 min) MOR catalyst series.

	MOR	MOR-al(0.2/70)	MOR-al(0.2/70)ac	MOR-al(0.4/85)	MOR-al(0.4/85)ac
X (mol%)	41.6	56.9	43.4	37.5	39.6
A ($\text{mol. h}^{-1} \text{g}^{-1}$)	0.96	1.50	1.01	0.84	0.92
TOF (h^{-1})	908	2049	1488	2484	1739

Table 6

Initial products distribution at ca 60% conversion on the fresh (time-on-stream, TOS = 2 min) MOR series.

	MOR	MOR-al(0.2/70)	MOR-al(0.2/70)ac	MOR-al(0.4/85)	MOR-al(0.4/85)ac
τ (h^{-1})	0.012	0.006	0.012	0.012	0.012
X (mol%)	61.3	56.9	57.8	53.7	58.9
Distribution (mol.%)					
Benzene	1.6	1.1	2.0	1.2	1.5
Toluene (T)	25.5	23.1	25.7	23.2	23.8
p-xylene	23.7	24.5	21.8	23.5	22.8
o-xylene	22.6	23.2	21.0	22.9	21.2
TMB	24.3	25.4	26.4	26.2	28.5
TeMB	2.1	2.7	2.9	2.9	2.2
Isom. (%)	46.3	47.7	42.9	46.4	44.0
p/o	1.04	1.05	1.04	1.03	1.07
Disp. (%)	53.6	52.3	58.1	54.6	56.0
I/D	0.86	0.91	0.75	0.86	0.78
T/TMB	1.06	0.90	0.97	0.88	0.83
1,2,3/1,3,5-TMB	0.34	0.33	0.32	0.35	0.27
Bimol. isom. (%) ^a	14.8	13.4	15.6	16.6	12.0

^a Contribution of bimolecular isomerization, estimated by method described in Ref. [31]. TMB and TeMB: trimethylbenzene and tetramethylbenzene respectively.

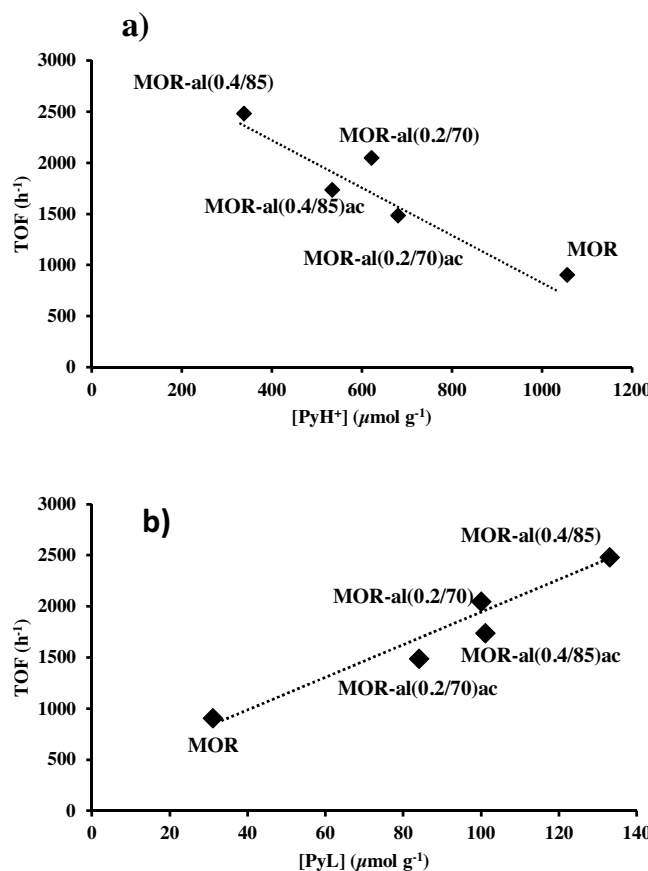


Fig. 7. Turnover frequency in m-xylene conversion as function of concentration of Brønsted (a) and Lewis acid (b) sites.

treatment widens the micropores of mordenite zeolite (both large canals and side pockets). Indeed N₂ adsorption shows formation of supermicropores (Table 2).

Main properties of spent catalyst are given in Table 6 (i.e. coke content, residual porosity, residual acidity). The amount of coke formed on catalysts after 1 h of reaction is between 5 and 7 wt.%. On MOR and MOR-al(0.4/85) catalysts, 70% of initial acid sites are inaccessible to pyridine against the half on the other samples. The toxicity of coke (Tox), number of acid sites deactivated per coke molecules, can be estimated from the coke content and residual acidity and by assuming an average molar weight of coke of 200 g mol⁻¹ (value base on previous studies). On the starting material, Tox is higher than 1, meaning that deactivation mode occurs by pore blockage. A simple mild alkaline treatment leads to a change in the deactivation mode: poisoning (Tox = 1). This effect is accentuated by using more severe desilication operating conditions and to a

lesser extent by a subsequent acid leaching (Tox < 1). On hierarchical MOR zeolites, coke is located both on mesopores and micropores (Table 7).

4. Conclusion

Desilication of mordenite zeolite with Si/Al ratio of 10 is performed by using sodium hydroxide. To obtain a significant mesoporosity with preservation of both crystallinity and micro-porosity, severe conditions are necessary (0.4 M and 85 °C, 2 h). Partial silicon extraction leads to formation of extra-framework aluminum species (EFAL) that a simple mild acid leaching can dissolve them. Concentration of Brønsted (BAS) acid sites, probed by pyridine at 150 °C, decreases after an alkaline treatment. That is not only due to a blocking effect of EFAL species, since after acid leaching BAS concentration is partially restored. The presence of the extraframework aluminum and also silicon induced the formation of weak OH bridged evidenced by CO adsorption at -100 °C.

Reactivity of *m*-xylene reveals that presence of EFAL reduces the space close to the acid sites, and also increases the strength of BAS. The synergic effect between BAS and LAS is demonstrated by the proportionality between concentration of LAS and TOF. Coke formation deactivates exclusively the reaction demanding more space as disproportionation reactions.

Acknowledgment

The authors would like to acknowledge the support provided by Algerian and French governments for funding this work through project Tassili No. 12-MDU/859. The support of Faculty Exact Sciences, Abderrahmane Mira University of Bejaia is gratefully acknowledged.

References

- J. Čejka, Introduction to Zeolite Science and Practice, In: H. van Bekkum, A. Corma, F. Schüth (Eds.), Elsevier Amsterdam, Studies in Surf. Sci. Catal. 168 (2007) 1.
- W. Vermeiren, J.-P. Gilson, Top. Catal. 52 (2009) 1131.
- M. Guisnet, J.-P. Gilson (Eds.), Zeolites for Cleaner Technologies, Imperial College Press, London, 2002.
- V. Valtchev, G. Majano, S. Mintova, J. Pérez-Ramírez, Chem. Soc. Rev 42 (2013) 263.
- M. Guisnet, P. Magnoux, Appl. Catal. 54 (1989) 1.
- A. Chica, A. Corma, J. Catal. 187 (1999) 167.
- T. Terlouw, J.-P. Gilson, European Patent 458 378 (1991), to Shell Int. Res. Mij. B.V.
- M.-C. Silaghi, C. Chizallet, P. Raybaud, Microporous Mesoporous Mat. 191 (2014) 82.
- C. Mirodatos, D.J. Barthomeuf, J. Chem. Soc. Chem. Commun. (1981) 39.
- C. Mirandatos, B.H. Ha, K. Otsuka, D. Barthomeuf, Proceedings of the 5th International Conference on Zeolites, In: Rees, (ed.), Heyden, London, 382 (1980).
- R. Szostak, Introduction To Zeolite Science and Practice, In: H. van Bekkum, E.M. Flanigen, P.A. Jacobs, J.C. Jansen (eds.), Elsevier Amsterdam, Stud. Surf. Sci. Catal. 137 (2001) 261.

Table 7
Properties of spent catalysts.

	Unity	MOR	MOR-al(0.2/70)	MOR-al(0.2/70)ac	MOR-al(0.4/85)	MOR-al(0.4/85)ac
Coke	wt.%	7.1	6.0	6.8	5.7	5.8
[PyH ⁺]	μmol g ⁻¹	309	314	367	92	298
[PyL]	μmol g ⁻¹	36	75	64	86	100
[PyH ⁺]/[PyH ⁺] ₀	–	0.30	0.51	0.53	0.27	0.56
[PyL]/[PyL] ₀	–	0.94	0.75	0.76	0.64	0.99
Tox ^a	–	2.08	1.01	0.94	0.86	0.80
V _{mic}	cm ³ g ⁻¹	0.15	0.13	0.16	0.10	0.17
V _{mes}	cm ³ g ⁻¹	0.06	0.11	0.12	0.21	0.21
(V/V ₀) _{mic}	–	0.75	0.69	0.76	0.64	0.95
(V/V ₀) _{mes}	–	0.95	0.78	1	0.90	0.80

^a Toxicity of coke Tox = (1 - ([PyH⁺]/[PyH⁺]₀)) / ([coke]/[PyH⁺]₀), [coke] is molar concentration of coke estimated by supposing an average molar weight of 200 g mol⁻¹.

- [12] D. Barthomeuf, *J. Phys. Chem.* 83 (1979) 249.
- [13] C.A. Henriques, J.L.F. Monteiro, P. Magnoux, M. Guisnet, *J. Catal.* 172 (1997) 436.
- [14] A. Corma, In: *Zeolites: Facts, Figures, Future*, P.A. Jacobs, R.A. Van Santen (eds.), Elsevier Amsterdam, *Stud. Surf. Sci. Catal.* 49 (1989) 49.
- [15] A. Corma, H. Garcia, *Chem. Rev.* 102 (2002) 3837.
- [16] P. Wu, T. Komatsu, T. Yashima, *J. Chem. S.O.C. Faraday Trans* 92 (5) (1996) 861.
- [17] Y. Hong, V. Gruver, J.J. Fripat, *J. Catal.* 150 (1994) 421.
- [18] D. Verboekend, J. Pérez-Ramírez, *Catal. Sci. Technol.* 1 (2011) 879.
- [19] V. Paixão, R. Monteiro, M. Andrade, A. Fernandes, J. Rocha, A.P. Carvalho, A. Martins, *Appl. Catal. A* 402 (2011) 59.
- [20] V. Paixão, P. Carvalho, J. Rocha, A. Fernandes, A. Martins, *Microporous Mesoporous Mater.* 131 (2010) 350.
- [21] M. Guisnet, P. Ayrault, J. Datka, *Pol. J. Chem.* 71 (1997) 1455.
- [22] A. Zecchina, G. Spoto, S. Bordiga, *Phys. Chem. Chem. Phys.* 7 (2005) 1627.
- [23] O. Marie, P. Massiani, F. Thibault-Starzyk, *J. Phys. Chem. B* 108 (2004) 5073.
- [24] M. Maache, A. Janin, J.C. Lavalle, E. Benazzi, *Zeolites* 15 (1995) 507.
- [25] K. Góra-Marek, K. Tarach, J. Tekla, Z. Olejniczak, P. Kuśtrowski, L. Liu, J. Martinez-Triguero, F. Rey, *J. Phys. Chem. C* 118 (2014) 28043.
- [26] S. Bordiga, C. Lamberti, F. Bonino, A. Travert, F. Thibault-Starzyk, *Chem. Soc. Rev.* 44 (2015) 7262.
- [27] N.S. Nesterenko, F. Thibault-Starzyk, V. Montouillout, V.V. Yuschenko, C. Fernandez, J.-P. Gilson, F. Fajula, I.I. Ivanova, *Microporous Mesoporous Mater.* 71 (2004) 157.
- [28] E.A. Pauktis, E.N. Yurchenko, *Usp. Khim.* 52 (1983) 426.
- [29] M. Rozwadowski, J. Datka, M. Lezanska, J. Włoch, K. Erdmann, J. Kornatowski, *Phys. Chem. Chem. Phys.* 3 (2001) 5082.
- [30] M. Guisnet, N.S. Gnepp, S. Morin, *Microporous Mesoporous Mater.* 35–36 (2000) 47.
- [31] S. Morin, N.S. Gnepp, M. Guisnet, *J. Catal.* 159 (1996) 296.
- [32] J.A. Martens, J. Perez-Pariente, E. Sastre, A. Corma, P.A. Jacobs, *Appl. Catal. A* 45 (1988) 85.